frontiers | Frontiers in Soft Matter

TYPE Original Research
PUBLISHED 12 January 2023
DOI 10.3389/frsfm.2022.1101680

OPEN ACCESS

EDITED BY
Abbas Rahmati,
University of Isfahan, Iran

REVIEWED BY
Weixiang Sun,
South China University of Technology, China
Fangfu Ye,
Institute of Physics (CAS), China

*CORRESPONDENCE
Qingsong Ye,
qingsongye@hotmail.com
Bae Hoon Lee,
bhlee@wiucas.ac.cn

SPECIALTY SECTION
This article was submitted to Gels, a section of the journal Frontiers in Soft Matter

RECEIVED 18 November 2022
ACCEPTED 28 December 2022
PUBLISHED 12 January 2023

CITATION
Yin H, Zhu M, Wang Y, Luo L, Ye Q and Lee BH (2023), Physical properties and cellular responses of gelatin methacryloyl bulk hydrogels and highly ordered porous hydrogels.
Front. Soft. Matter 2:1101680.
doi: 10.3389/frsfm.2022.1101680

Physical properties and cellular responses of gelatin methacryloyl bulk hydrogels and highly ordered porous hydrogels

Haiyan Yin[1,2], Mengxiang Zhu[1], Yingying Wang[1], Lihua Luo[3], Qingsong Ye[3]* and Bae Hoon Lee[1,2]*

[1]Wenzhou Institute, University of Chinese Academy of Sciences, Wenzhou, Zhejiang, China, [2]Oujiang Laboratory (Zhejiang Lab for Rengerative Medicine Vision and Brain Health), Wenzhou, Zhejiang, China, [3]School and Hospital of Stomatology, Wenzhou Medical University, Wenzhou, Zhejiang, China

Protein-based hydrogels hold a high content of water in their three-dimensional (3D) network structure and exhibit innate biological activities as well as soft tissue-like mechanical properties, resulting in being highly applicable to various tissue engineering fields. However, precisely controlling the 3D porous structure of protein-based hydrogels remains a challenging task, and understanding the influence of their porous structure on physical properties and cellular responses is crucial for tissue engineering applications. In this study, we prepared highly ordered gelatin methacryloyl hydrogels with regular interconnected pores and traditional bulk hydrogels with irregular pores to evaluate their differences in physiochemical properties and cellular behaviors. Highly ordered gelatin methacryloyl hydrogels exhibited a high degree of compliance owing to their sponge-like structure whereas gelatin methacryloyl bulk hydrogels exhibited relatively higher moduli but were brittle due to a densely packed structure. The highly ordered gelatin methacryloyl hydrogels with interconnected pores supported higher cell viability (about 100%) due to an efficient flux of oxygen and nutrients compared to the dense bulk hydrogels showing cell viability (around 80%). Also, cells in the highly ordered gelatin methacryloyl hydrogels displayed a more stretched morphology compared to those in the gelatin methacryloyl bulk hydrogels that exhibited a more round morphology during the cell culture period.

KEYWORDS

gelatin methacryloyl (GelMA), highly ordered GelMA hydrogels, bulk hydrogels, human dental pulp stem cells (hDPSCs), 3D cell culture

Introduction

Recently cell culture has shifted from 2D towards 3D culture systems because 3D culture systems can more closely recapitulate the *in vivo* microenvironments owing to enhanced cell-cell and cell-matrix interactions (Pampaloni et al., 2007). Several methods and technologies have been used for 3D culture: hydrogels (Andersen et al., 2015), bioreactors (Wendt et al., 2009), sandwich (Reif et al., 2015), hanging drop (Bartosh and Ylostalo, 2014), microfluidic platforms (Wang et al., 2015; Liu et al., 2017), bioprinting (Matai et al., 2020), etc. These methods allow for the formation of 3D cell constructs (e.g., spheroids and multi-cell sheets) that can promote cell-cell interactions, leading to *in vivo*-like cellular responses. However, for bioreactors, microfluidic platforms, and bioprinting, special instruments are required; the hanging drop culture elicits the occurrence of necrotic areas in the center of spheroids; the sandwich culture limits cell-cell interactions, making it suitable only for short-time cell culture.

Relative to the other culture systems, 3D hydrogel systems may present a more biological microenvironment to cells because hydrogels are close to human tissues that contain 70%–80% water. Furthermore, hydrogels have good biocompatibility, controllable mechanical properties, and a similarity to the extracellular matrix structure, thus being recognized as potential biological matrices (Naderi-Meshkin et al., 2014; Lee et al., 2015; Lu et al., 2015).

Protein-based hydrogels are especially useful for cell encapsulation and tissue regeneration applications because they have innate biological signal cues to promote cell-ECM interactions and furthermore direct cellular behaviors. Although commercially available Matrigel® provides in vivo-like environments for 3D cell culture, it has drawbacks including batch-to-batch variations and immune responses due to composition complexity and extraction source contaminants (Aisenbrey and Murphy, 2020). In recent years, several kinds of protein-based hydrogels such as collagen (Parenteau-Bareil et al., 2010) silk fibroin (Kim et al., 2004) gelatin (Jaipan et al., 2017) and serum albumin (Tang et al., 2018) have been used for 3D cell culture and tissue regeneration applications. Among these materials, gelatin is one of the most popular/affordable protein/peptide materials for fabrication of protein-based hydrogels. Like collagen, gelatin contains the tripeptide Arg-Gly-Asp (RGD) sequence for cell adhesion and the matrix metalloprotease (MMP) targeting sequence, which is beneficial to cell remodeling (Wang et al., 2016). However, the weak mechanical properties of gelatin in aqueous solutions at body temperature can be a barrier for 3D cell culture and tissue engineering applications. An Van Den Bulcke (Van Den Bulcke et al., 2000) et al. proposed and prepared gelatin methacrylamide hydrogels (GelMA: gelatin methacryloyl; gelatin methacrylate) for the first time; GelMA offers a fast and efficient photo-crosslinking process upon exposure to UV light in the presence of photo-initiators. Thus, GelMA can easily form hydrogels with controllable mechanical properties depending on the concentration of GelMA, the degree of methacryloylation, the concentration of photo-initiators, and light intensity. Additionally, GelMA retains the functional amino acid sequences of gelatin such as RGD polypeptide sequence and MMP degradation sequence, offering cell adhesion and remodeling environments (Khayat et al., 2017; Yin et al., 2018). Therefore, cell laden-GelMA hydrogels have been widely utilized for engineering 3D tissue replicas for various bio-applications such as tissue engineering (Klotz et al., 2016) "bio-ink" for 3D bioprinting (McBeth et al., 2017) and regenerative medicine (Annabi et al., 2014).

In recent years, it has been reported that cell-laden GelMA hydrogels can regulate cell behaviors (Nichol et al., 2010; Yue et al., 2015; Zhao et al., 2016) such as proliferation, migration, and differentiation in different 3D culture systems. Thus, GelMA 3D hydrogel scaffolds have been used as ideal candidates in fields of tissue engineering and drug delivery. However, there are still certain challenges in accurately controlling the porosity, pore size, and interconnectivity of GelMA hydrogels. Hydrogels differ in pore architecture depending on preparation methods. They can be non-porous or macroporous (10–500 μm) (Li and Mooney, 2016). The pore size of dried bulk hydrogel (with non-porous structure on visual observation) scaffolds is generally smaller than 10 μm, which can limit cell infiltration, tissue growth, and blood vessel formation of tissue engineering constructs (Sedlačík et al., 2020). On the other hand, macroporous hydrogels with interconnected pores can be compressed in large volumes. Currently, a variety of methods have been established to prepare the macroporous hydrogels, including the porogen template method (Huebsch et al., 2015), cryogelation (Koshy et al., 2014), gas pore method (Dehghani and Annabi, 2011; Wang et al., 2014), and mechanical porogen method (Wang et al., 2018). These macroporous hydrogels can be compressed to lower than 10% of their standing volume during injection, and quickly restore their original volume and shape after being separated from the injection device. Compared with bulk hydrogels, macroporous hydrogels have some unique advantages, including shape memory, ease of use, and controllable physical and chemical properties. Recently, some researchers have paid attention to the inverted colloidal crystal hydrogels that regulate cell behaviors. Kotov's group demonstrated that ICC hydrogels with a hexagonal structure with interconnected regular pores can enhance cell-cell and cell-ECM interactions and can be used for three-dimensional cell culture (Kotov et al., 2004; Nichols et al., 2009) However, most current ICC scaffolds are made of non-biodegradable artificial polymers such as polyacrylamide (da Silva et al., 2010), poly (ethylene glycol) (Stachowiak and Irvine, 2008), poly (hydroxyethyl methacrylate) (Long et al., 2013) and N-isopropylacrylamide (NIPAM) (Shao et al., 2019), limiting their application in biomedical fields. To address this limitation, Xia et al. reported the use of biodegradable synthetic poly (lactic acid-hydroxyacetic acid) ICC scaffolds for tissue engineering applications. However, synthetic biodegradable scaffolds have lack of biological functions for the regulation of cell-ECM interactions (Choi et al., 2013; Zhang et al., 2014). In order to solve this issue, they further modified the surface of ICC scaffolds prepared from PEGDA (poly (ethylene glycol) diacrylate) using collagen that mimics the extracellular matrix, allowing cell to adhere to the cavity wall, resulting in significantly improved cell-cell and cell-ECM interactions. Although these studies have demonstrated the importance of combining ICC scaffold technology and protein modification technology for 3D cell culture, there are still some technical difficulties to overcome, such as the cytotoxicity of degradation by products of some synthetic materials and the tedious operation of protein modification. In this regard, GelMA-based ICC scaffolds have some advantages such as cell-adhesion capability without protein modification, biodegradation, controlled mechanical properties, and controlled regular pore structure (Lee et al., 2017).

There are two types of GelMA-based hydrogels that have been used as 3D scaffolds for various bioapplications. One is GelMA bulk hydrogel with a random pore structure that is studied in most of the GelMA research whereas the other is inverted colloidal crystal (ICC) GelMA hydrogel with a regular pore structure that has been recently developed (Lee et al., 2017). To the best of our knowledge, there is no report of the effect of pore regularity of GelMA hydrogels on cell behavior. In this work, we studied the influence of the pore structure of two different GelMA hydrogels (GelMA bulk scaffolds and ICC scaffolds) on physical properties, mechanical properties, and dental pulp stem cell behaviors in 3D cell culture system (Scheme 1).

Experiments

Materials

Gelatin (type B, 100 and 250 blooms, Aladdin Shanghai, China), sodium carbonate, sodium bicarbonate decahydrate, sodium

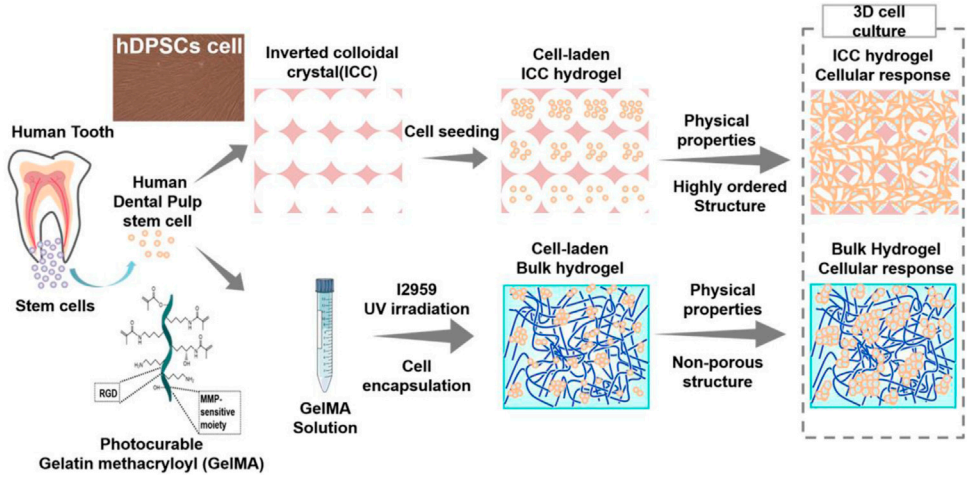

SCHEME 1
Schematic illustration of cell encapsulation in GelMA bulk hydrogels and cell seeding on the GelMA ICC hydrogels.

hydroxide, acetohydroxamic acid, hydroxylamine, sodium dodecyl sulfate, and alanine were purchased from Aladdin (Shanghai, China). Methacrylic anhydride (MAA), 2-hydroxy-4'-(2-hydroxyethoxy)-2-methylpropiophenone (I2959), and collagenase (‖, 125 CDU/mg) were purchased from Sigma-Aldrich (Shanghai, China). Deuterium oxide (D_2O) and 2,2,3,3-D_4 (D, 98%) sodium-3-trimethylsilylpropionate (TMSP) were obtained from Cambridge Isotope Laboratories (Andover, United States). Human dental pulp stem cells (hDPSCs) were received from Wenzhou Medical University (Luo et al., 2021) Dulbecco's Modified Eagle's Medium, fetal bovine serum, Hanks' Balanced Salt Solution (HBSS) (10X), penicillin/streptomycin, and Live/Dead® Cell Viability/Cytotoxicity kit were purchased from Life Technologies (Shanghai, China). All the reagents were used as received.

Fabrication of GelMA ICC and GelMA bulk hydrogel scaffolds

GelMA samples were synthesized according to the literature (Shirahama et al., 2016). Briefly, type B gelatin (100 and 250 blooms) was dissolved at 10 w/v% at 50°C in .25 M carbonate-bicarbonate [CB] buffer). GelMA samples were prepared by reacting gelatin with methacrylic anhydride (MAA, 94%) at a feed ratio of MAA (60 mL) to gelatin (100 g) at 50°C for 2 h in CB with pH maintenance at 9.0 in a time-lapse loading manner. After the 2 h reaction, the solutions were readjusted to pH of 7.4, filtered, dialyzed using PALL Minimate TFF Capsule with 10 kDa MWCO at 50°C for 1 day, lyophilized, and stored at −20°C until further use. The degree of substitution (DS) of GelMA was verified by ^{1}H-NMR (Avance I 400MHz, Bruker) in deuterium oxide. For ^{1}H-NMR testing about gelatin and GelMA, 20 mg of each sample was dissolved in 800 μL of deuterium oxide with .1 w/v% TMSP as an internal reference at 40°C. The DS calculation was performed according to the previous literature (Zhu et al., 2019).

For GelMA ICC hydrogels, polystyrene beads with a diameter of 138 ± 2.0 μm (Duke Scientific Corporation) dispersed in a 70% ethanol solution were self-assembled in 6 mm-diameter polypropylene molds by shaking for 48 h and annealed at 134°C for 6 h to obtain lattices. GelMA samples were dissolved at 30 w/v% in distilled water at 50°C. Then, GelMA solutions containing .5 w/v% 2-Hydroxy-4'-(2-hydroxyethoxy)-2-methylpropiophenone (I2959) were infiltrated into the lattices by centrifugation at 15,000 rpm at 40°C for 10 min. The GelMA-infiltrated lattices were cured by ultraviolet light (UV; 365 nm at 50 mW/cm^2) for 10 min, and then the polystyrene lattices were removed in tetrahydrofuran. The PS beads were soaked into THF and removed by multiple changes of a THF solution. During the THF treatment, PS beads dissolved in THF quickly; however, ICC GelMA hydrogels did not dissolve in THF and instead exchanged some part of water with THF. ICC GelMA gels were shrunk partially during the THF process but they recovered their original shape in aqueous solutions. The resultant GelMA ICC scaffolds were sterilized with a 70% ethanol solution and washed three times with PBS, finally being stored in distilled water or PBS at 4°C until further use. GelMA bulk hydrogels were prepared in the polypropylene molds with a diameter of 6 mm under the low power of photocuring conditions (UV; 365 nm at 4 mW/cm^2) without the templating of polystyrene beads.

Swelling kinetics and Porosities of GelMA hydrogel scaffolds

GelMA ICC and bulk hydrogels were freeze-dried for 3 days using a freeze dryer. In order to evaluate their swelling kinetics, each freeze-dried sample was immersed in a DPBS solution to measure the weight of each sample over time. The swelling ratio was calculated by the following equation:

$$\textit{Swelling ratio} = \frac{Wi}{Wd} \quad (1)$$

Where Wi is the weight of the swollen sample and Wd is the weight of the freeze-dried sample.

The porosity of GelMA ICC hydrogels and bulk hydrogels was characterized by acquiring the weight of swollen scaffold W_i and the weight of freeze-dried macro- and microporous hydrogel scaffolds W_d.

For scaffolds with large porosity, following Du's opinion (Jiang et al., 2019) the porosity can be calculated according to the equation:

$$\textbf{\textit{Porosity}} = \frac{\textbf{\textit{Wi}} - \textbf{\textit{Wd}}}{\textbf{\textit{Wd}}} \quad (2)$$

Compressive tests

For compression testing, GelMA bulk hydrogels and ICC hydrogels were prepared by the previous method using 30 w/v% GelMA containing .5 w/v% I2959 through the UV photopolymerization. GelMA bulk hydrogels and ICC hydrogels with a diameter of 4–5 mm and a thickness of 4 mm were fabricated and tested using a universal mechanical testing machine (UTM2102; Shenzhen, China). The speed of the crosshead was .25 mm s^{-1}. The compression strain and stress were recorded until the hydrogel was crushed. The compressive modulus was determined as the slope of the stress-strain curve from 0 to .15 mm/mm strain. The modulus of the porous material, E, can be related to the modulus of the non-porous hydrogel (E_0) by the following equation, where the porosity is assigned the variable (Welzel et al., 2012; Welzel et al., 2014; Sedlačík et al., 2020), p:

$$\boldsymbol{E = E_0 \cdot (1 - p)^2} \quad (3)$$

Rheological measurements

Mechanical properties of aqueous GelMA solutions (30 w/v%) containing I2959 (.5 w/v%) were characterized by sinusoidal shear rheometry. Frequency-sweep measurements were conducted using a rheometer (TA DHR-2). The storage moduli of GelMA ICC and bulk hydrogels were measured with an 8 mm parallel-plate geometry at .1% strain and .1 Hz at 37°C throughout the measurements. Mesh size of the GelMA bulk hydrogel was calculated according to the following equation (Lee et al., 2017). Where G' is the storage modulus, N_A is the Avogadro constant, R is the molar gas constant, and T is the temperature.

$$\boldsymbol{\xi = \left(\frac{G' \cdot N_A}{RT}\right)^{-\left(\frac{1}{3}\right)}} \quad (4)$$

Accelerated enzyme degradation study

ICC and bulk hydrogels made of GelMA (30 w/v%) were tested for enzymatic degradation in 2 mg/mL of collagenase type Ⅱ (125 CDU/mg solid) in Hank's Balanced Salt Solution (HBSS), containing 3 mM $CaCl_2$. Surface morphology of the GelMA ICC hydrogels and GelMA hydrogels was observed by optical microscopy. For each degradation time point, gross images were taken, and mass loss of GelMA ICC and GelMA bulk hydrogels was simultaneously measured. The initial swollen weight (W_i) of each hydrogel sample (n = 5) was measured, and then each hydrogel sample was put into a 2 mg/mL collagenase type Ⅱ solution and was incubated at 37°C. At each degradation time point, each sample was taken out and washed with HBSS solution 3 times, and the excess surface water was removed using Kim-wipes, and the degraded weight (W_d) of each sample was recorded again.

$$\textbf{\textit{Mass loss}}\ (\%) = \frac{\textbf{\textit{Wi}} - \textbf{\textit{Wd}}}{\textbf{\textit{Wi}}} \quad (5)$$

Cell culture

Human dental pulp stem cells (hDPSCs) were maintained in alpha-MEM Dulbecco's Modified Eagle's Medium (Hyclone) with 10% fetal bovine serum (Hyclone) and 1% penicillin/streptomycin (Life Technologies) in a humidified atmosphere at 37°C with 5% CO_2. The medium was changed every 2–3 days. The hDPSCs and protocols were independently reviewed and approved by the Ethics Committee of the School and Hospital of Stomatology, Wenzhou Medical University (No. WYKQ2018008SC) (Luo et al., 2021). Before cell seeding, GelMA ICC scaffolds were placed in 24-well plates, consequently washed with PBS and kept in 2 mL media for 30 min before cell loading. After media aspiration, 1×10^5 cells in 10 μL of medium were carefully pipetted on top of each GelMA ICC scaffold. Also, for cell encapsulation of GelMA bulk hydrogels, 1×10^5 cells were mixed with a 30 w/v% GelMA solution of 40 μL (.5 w/v%) and cured by 365 nm UV for 5 min (UV; 365 nm at 4 mW/cm^2). After 4 h, the cell-encapsulated scaffolds were transferred into a new 24-well plate with 1 mL of media. For both cell-laden hydrogel systems, the media were changed every 2–3 days. The loading efficiency of each GelMA system was measured by counting the real number of loaded cells after treating cell-laden hydrogels with .25% trypsin/EDTA solution *via* measuring the unloaded cells in each well (N = 3).

Viability and proliferation assays of human dental pulp stem cells (hDPSCs) within GelMA bulk hydrogels and ICC hydrogels

Cell viability in GelMA ICC hydrogels and GelMA bulk hydrogels was measured by the cell counting Kit-8 (CCK-8, Donjindo Molecular Technologies) assay according to the manufacturers' protocol. To test the O. D value, a 400 μL CCK-8 solution (1:10 dilution to culture media) was added to each sample at different culture time (1day, 7 days, and 21 days), each sample was incubated for 4 h at 37°C, and the absorbance was measured at 450 nm.

Cell viability in 3D GelMA ICC scaffolds and 3D GelMA bulk scaffolds were characterized using LIVE/DEAD® Cell Viability/Cytotoxicity kit (Life Technologies). Briefly, 4 μM Calcein-AM and 8 μM ethidium homodimer-1 (EthD-1) in media were added to the samples, followed by incubation of 1 h at 37°C. The cytoplasm of live cells and nucleus of dead cells were stained by Calcein-AM (green) and EthD-1 (red), respectively and observed with a confocal microscope (Nikon, A1, Japan). The number of living and dead cells were counted using ImageJ.

Morphological characterization

To investigate cell morphology inside of hydrogels, F-actin of cells in each hydrogel sample was stained by Alexa Flour® 488 labeled phalloidin (Life Technologies). The nuclei of cells

were stain by 4,6-Diamidino-2-Phenylindole Dihydrochloride (DAPI; Life Technologies). The samples were washed twice with PBS, and fixed with 4% paraformaldehyde (PFA) for 5min, then permeabilized with .1% Triton X-100 for 30min, washed with PBS twice, and incubated in 3% BSA blocking buffer for 1 h. Alexa Flour® 488 was then added to label phalloidin to each sample by reacting for 2 h at room temperature, followed by washing twice with PBS. Finally, sample stain by 10ug/ml DAPI for 10 min, before being imaged using a confocal microscope. The roundness and aspect ratio were measured using ImageJ.

$$Roundness = \frac{4\pi \cdot area}{(convex\ perimeter)^2} \quad (6)$$

$$Aspect\ ratio = \frac{Length}{Width} \quad (7)$$

To investigate the microscopic morphology of cells in hydrogels, scanning electron microscopy (SEM) was utilized. Samples were fixed with 4% PFA and were treated by sequential ethanol dehydration at 25, 50, 75, 95, and 100% for 15 min each. The scaffolds were frozen at −80°C, followed by lyophilization for 3 days. The SEM samples were coated by Pt with a thickness of 10 nm using a sputter coater (Leica, EM ACE600, Germany), and their images were taken with a field emission scanning electron microscope (HITACHI, SU8010, Japan) at an acceleration voltage of 5 kV.

Calculation of RGD motif density in the GelMA ICC and bulk hydrogel

RGD motif is known to mediate cell attachment on the gelatin scaffolds. The RGD motif in the different GelMA hydrogel systems was calculated *via* Du's method (Jiang et al., 2019). A GelMA scaffold in the size of π *3²*1 (mm^3) is made of 4 mg of gelatin: the total molecular number of RGD motif in the scaffold can be estimated as follows (where N_A is defined as Avogadro constant):

$$N_{RGD} = \frac{Weight_{GelMA}}{MW_{procollagen}} \times 7 \times N_A \quad (8)$$

Considering the porosity of 95%, the volume for gelatin inside can be calculated:

$$V_{GelMA} = V_{Scaffold} \times (1 - p) \quad (9)$$

The average volume containing one single RGD motif would be estimated as:

$$V_{RGD} = \frac{Vgelatin}{N_{RGD}} \quad (10)$$

The average spacing between nearby RGD motifs would be estimated as:

$$Gap_{RGD} = \sqrt[3]{V_{RGD}} \quad (11)$$

Statistical analysis

Statistical analysis was performed using the Microsoft Excel statistical analysis software package. Comparisons between the two treatments were made using a two-tailed pair Student's t-test. Two-way ANOVA was used to test for differences among at least three groups. The standard deviation was calculated and presented for each treatment group (mean ± SD). Results with a *p*-value of below .05 were considered statistically significant. (*: $p < .05$; **: $p < .01$; ***: $p < .001$; ****: $p < .0001$).

Results and discussion

Synthesis of high DS GelMA

GelMA with a high degree of substitution was successfully prepared using our previous synthesis method (Shirahama et al., 2016; Zhu et al., 2019; Luo et al., 2021). Figure 1A shows that gelatin has amino and hydroxyl groups susceptible to react with methacrylic anhydride (MAA) to form methacrylamide groups and methacrylate groups, respectively. GelMA made of gelatin with a higher bloom number of 250 shows higher viscosity below 25°C (Figure 1B) as compared to GelMA made of gelatin with a lower bloom of 100. High viscous GelMA solutions can cause a handling issue during cell encapsulation process and ICC fabrication. GelMA with a lower bloom of 100 exhibited low viscosity over a wide range of temperature from 10°C to 40°C, which is suitable for the next stage of experiments (cell encapsulation and ICC microfabrication) (Figure 1B).

In this study, a high degree of modification was achieved (GelMA DS_{300}). The amount of methacryloylation (AM) of GelMA was quantified by ^{1}H-NMR (AM_{NMR}). ^{1}H-NMR was used to quantify both methacrylamide and methacrylate groups in GelMA (Yue et al., 2017; Zheng et al., 2018; Zhu et al., 2019). The ^{1}H-NMR spectra of GelMA, as compared with gelatin (Figure 1C) show new proton peaks (a+b + e) at 5.4–6.1 ppm. They correspond to the acrylic protons (CH_2 = C(CH_3) CONH-) of methacrylamide groups at 5.7–5.6 and 5.5–5.4 ppm (peaks a and b) and acrylic protons (CH_2 = C(CH_3)COO-) of methacrylate groups at small peaks at 6.1 and 5.7 ppm (peak e). In addition, GelMA also showed a peak at 1.9 ppm (peak d) for methyl protons (CH_2 = C(CH_3) COO- and CH_2 = C(CH_3)CONH-) of the methacryloyl groups, compared with gelatin. When the lysine group of gelatin was completely functionalized with MAA, the specific peak of the unreacted lysine group ($NH_2CH_2CH_2CH_2CH_2$-) at 3.0 ppm (peak c) completely disappeared. The quantified amount of methacryloyl groups in GelMA is summarized in the table in Figure 2C. The AM_{NMR} value of GelMA was 1.19 ± .02 mmol/g. According to the previous literature we calculated DS (the equation shows in Supplementary Figure S1) reached to 302.80%. Both the amino groups and the hydroxyl groups are susceptible to substitution, which is why the DS can be higher than 100%. We used GelMA with a higher DS that supported its denser crosslinking and longer stability as well as facilitated ICC fabrication process owing to its lower viscosity at room temperature.

Physical characterization

Characterization of hydrogel structure

Compared to 2D cell culture, 3D cell culture systems are closer to the *in vivo* micro-environments that more closely reflect the morphology and viability of cells in the body (Cukierman et al., 2001; Dutta and Dutta, 2009). Cellular encapsulation in 3D hydrogels was the most popular technique for the development of tissue regeneration (Khetan and Burdick, 2009; Liaw et al., 2018). Here

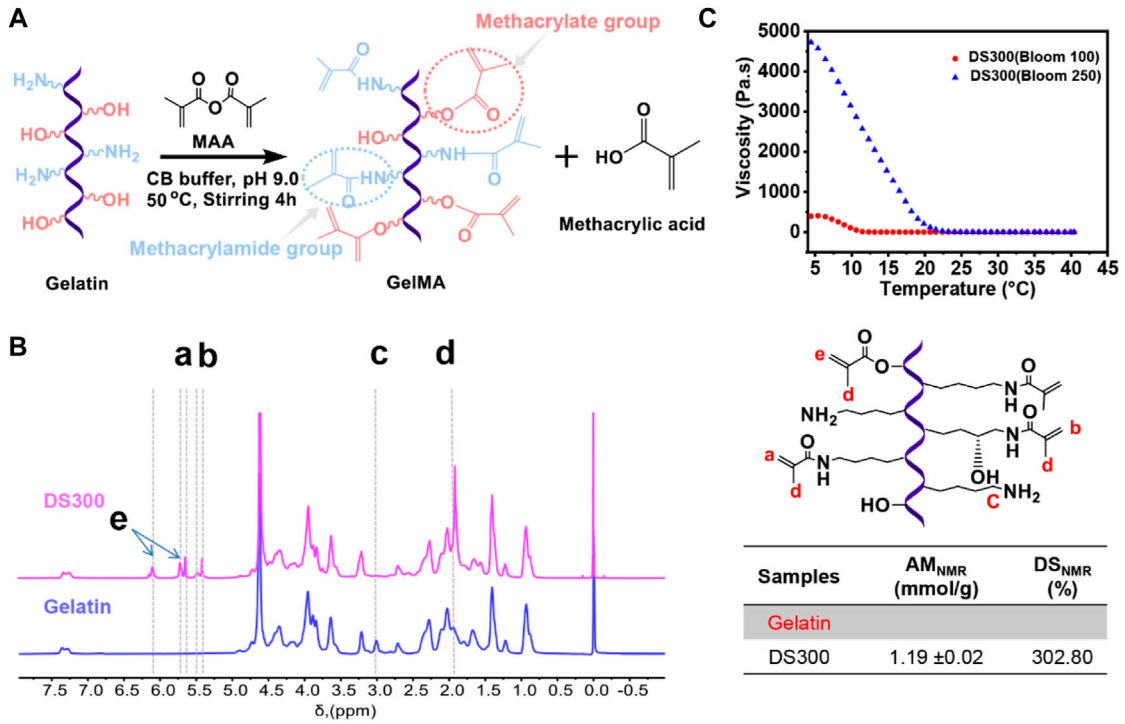

FIGURE 1
(A) Schematic illustration of GelMA (gelatin methacryloyl) synthesis *via* reaction of gelatin with methacrylic anhydride. **(B)** Viscosity of a GelMA solution (30 w/v%) at temperatures ranging from 4°C to 40°C with different blooms (blue line: 250 bloom, red line: 100 bloom). **(C)** ^{1}H NMR verification of gelatin and GelMA. Peaks correspond to acrylic protons (2H) of methacryloyl grafts of lysine groups and hydroxyl lysine groups ,(a, b), methylene protons (2H) of unreacted lysine groups **(C)**, methyl protons (3H) of methacryloyl grafts (d), and acrylic protons (2H) of methacrylated grafts of hydroxyl groups (e).

we examined the influence of different 3D network structural properties of 3D GelMA hydrogels on the morphology and viability of human dental pulp stem cells as model cells. *In situ* photo-polymerization (bulk hydrogels) and inverted colloidal crystal (ICC hydrogels) methods were used to fabricate 3D GelMA hydrogels with different porous network structures. From our previous work, ICC hydrogels made of 30 w/v% GelMA provided good structural stability (Lee et al., 2017). Therefore, in this study 30 w/v% GelMA was also used to compare bulk hydrogels and ICC hydrogels. The microstructure of two GelMA hydrogels in a dry state and wet state (Figure 2) was evaluated by scanning electron microscopy (SEM) and microscopy, respectively. Interestingly, the SEM image of GelMA bulk hydrogels exhibited an irregular porous structure (Figure 2A), and the small pores are separated by a thin wall. In contrast to GelMA bulk hydrogels, the SEM image of GelMA ICC hydrogels displayed regular pores (Figure 2B) that were interconnected by several small windows [Figure 2(b')]. For the quantitative analysis of the microstructure of GelMA bulk and ICC hydrogels, SEM images were further examined using ImageJ software. In GelMA bulk hydrogels, the average pore diameter was 5.42 ± 1.90 μm (Figure 2E), and their pores were distributed irregularly (Figure 2C). However, in GelMA ICC hydrogels, the average pore diameter was 99.8 ± 6.01 μm (Figure 2E), and their pores were distributed regularly (Figure 2D). The pore size of GelMA bulk hydrogels seemed to be much smaller than the size of a cell (near 10–20 μm), which would affect cell-cell interactions, migration, and nutrient diffusion throughout the scaffold (Shanbhag et al., 2005). However, the porous structure of GelMA ICC hydrogels possessed an interconnected networks with open windows (near 30–50 μm) that could be conducive to the infiltration of cells and the efficient diffusion of oxygen and nutrients throughout the scaffold (Shanbhag et al., 2005; Zhang et al., 2013; Lee et al., 2017). Also, the average mesh size of the bulk hydrogels was calculated from the rubber elasticity theory using Eq. 4, exhibiting a mesh size of about 6.86 ± .32 nm. The cross-linked polymeric network has a nanometer length-scale mesh size resulting in thin walls. To avoid the interference of quenching and freeze-drying on the microstructure of gels, we evaluated gels in a hydrated state by microscopy. GelMA bulk hydrogels had a smooth surface; they appeared to be non-porous in the hydrated state (Figure 2F). On the other hand, GelMA ICC hydrogels had a regular porous structure (Figure 2G) in the hydrated state. The pore size of ICC hydrogels in a freeze-dried state was smaller than that in the hydrated state (~124 μm) potentially owing to the shrinkage during the operation process.

Porosity and water absorption properties

From the porosity equation, the porosity of GelMA ICC and bulk hydrogels was separately calculated. The porosity of GelMA ICC hydrogels was 89.38 ± .01% whereas the porosity of GelMA bulk hydrogels was 72.93 ± .02% (Figure 3B). Relative to the porosity, the swelling kinetics of the hydrogels showed different performances (Figure 3A). After swelling in water for 10 min, both of the hydrogels showed a constant water absorption ability. GelMA ICC hydrogels exhibited 3 times higher water absorption ability than GelMA bulk hydrogels probably owing to their higher porosity and pore size. Such a swelling phenomenon was also observed in cryogels

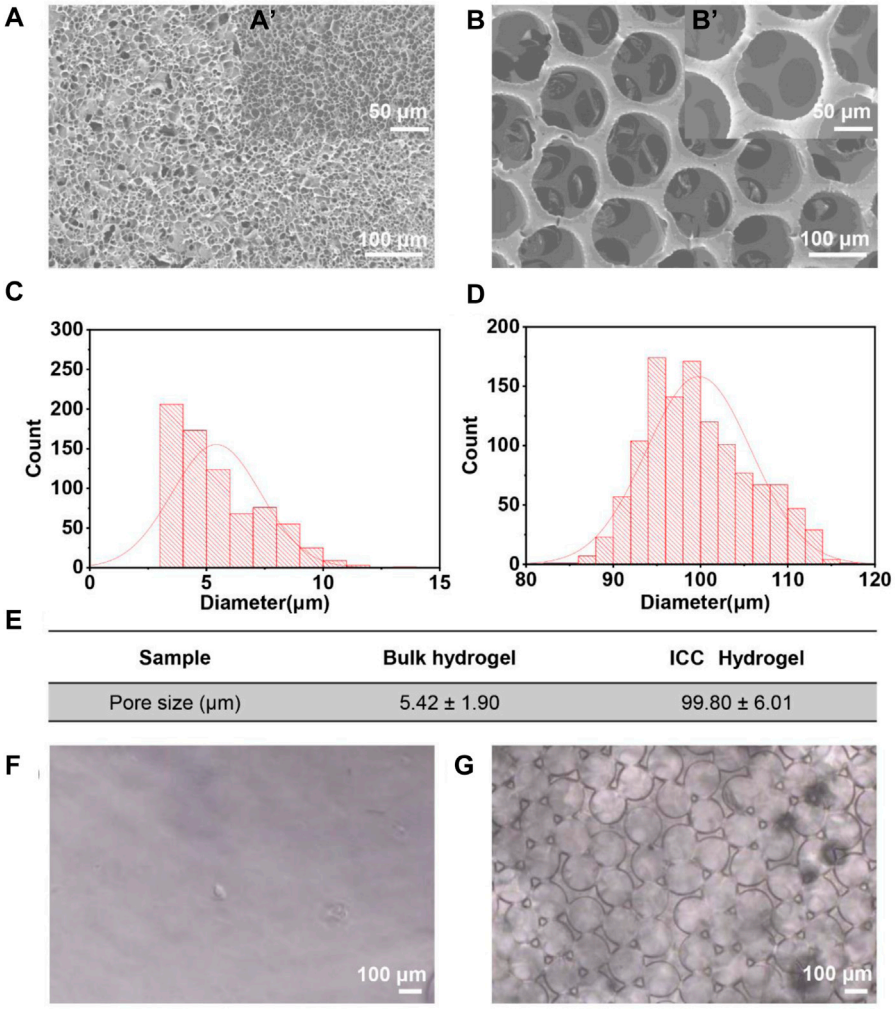

FIGURE 2
(A) SEM image of GelMA bulk hydrogels. (a`) Magnification images of GelMA bulk hydrogels. **(B)** SEM image of GelMA ICC hydrogels. (b`) High magnification image of GelMA ICC hydrogels. **(C,D)** Histogram of pore size (diameter) distribution of GelMA bulk and GelMA ICC hydrogels, respectively. **(E)** Analysis of pore size from the SEM images by ImageJ. **(F)** Microscope image of GelMA bulk hydrogels. **(G)** Microscope image of GelMA ICC hydrogels.

with macroporous structures (Wu et al., 2012). From the gross images of both of the hydrogels, GelMA ICC hydrogels appeared like a sponge [Figure 3(b")] whereas GelMA bulk hydrogels shaped like a jelly [Figure 3(b')]. Sponge-like ICC hydrogels had a macroporous structure with interconnectivity; their water absorption ability could depend on the capillary force. On the other hand, the jelly-like GelMA bulk hydrogels had a less porous structure; their water absorption ability could depend on the osmotic pressure.

Mechanical and Rheological properties of the 3D hydrogel

The network structure of 3D hydrogels influences mechanical properties and also affect swelling as well as mass flux throughout the matrix (Bertz et al., 2013; Caliari and Burdick, 2016; Santos et al., 2018). First, the effect of the network structure of hydrogels on mechanical properties was evaluated. When stress was applied to GelMA bulk and ICC hydrogels, their deformation phenomena were quite different (Figure 3C). For GelMA bulk hydrogels, the samples broke down after 35% strain was applied. Interestingly, GelMA ICC hydrogel samples could recover their original shape even after 90% strain was applied. From the results of the strain-stress curve (Figure 3D), the fracture stress of GelMA bulk hydrogels reached 1.6 MPa at 35% strain. However, in the case of GelMA ICC hydrogels, their mechanical fracture was not observed even after compression up to 90% strain. The Young's modulus of ICC hydrogel at the low strain region is almost linear elastic. When ICC hydrogels were compressed in the high strain regions, progressive collapse of the pores in the gels was caused by elastic buckling of the pore walls. In the meanwhile, water contained in the interconnected pore system flowed out from the scaffold. GelMA bulk hydrogels showed a Young′s modulus of 1.81 MPa whereas GelMA ICC hydrogels at the same polymer concentration exhibited a dramatic reduction in Young′s modulus (.029 MPa) (Figure 3D). From knowing the Young′s modulus of GelMA bulk hydrogel and the porosity of the porous GelMA ICC hydrogel, the expected Young's modulus of GelMA ICC hydrogels was calculated by Equation (3), (Welzel et al., 2012; Sedlačík et al., 2020). The calculated Young′s modulus of GelMA ICC hydrogel was .022 MPa, which is close to the experimental results. In summary,

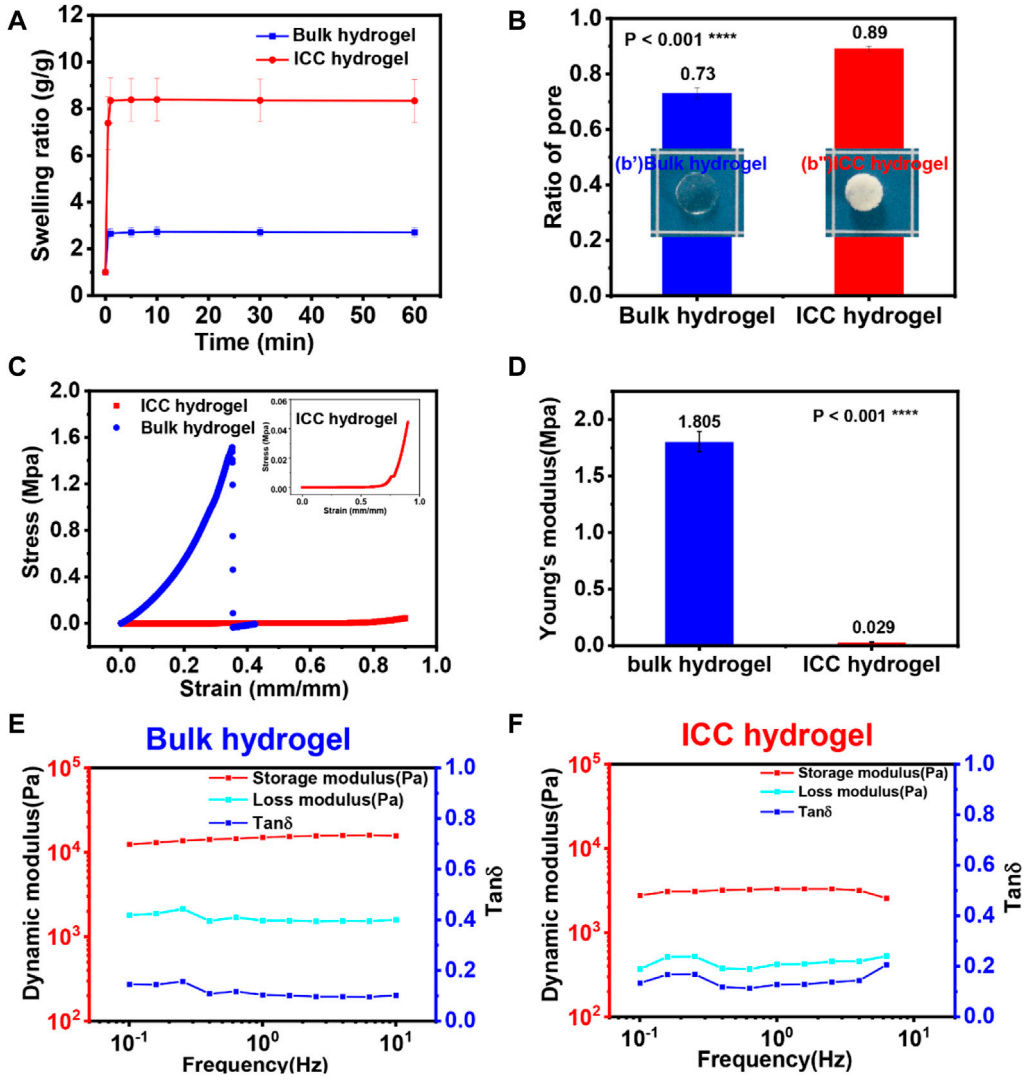

FIGURE 3
(A) Swelling kinetics of GelMA bulk and ICC hydrogels. **(B)** The ratio of pore of GelMA ICC and bulk hydrogels. (b') & (b") Images of GelMA bulk and ICC hydrogels **(C)** Strain-stress (S-S) curve of GelMA bulk hydrogels (blue) and GelMA ICC hydrogels (red). Inset image is the S-S curve of ICC hydrogels (red). **(D)** Young`s modulus was calculated from the strain-stress curve in the range of 0–.15 strain (right figure). Each sample was tested three times. **(E,F)** Storage modulus (G′), Loss modulus (G″) and tanδ of the GelMA bulk hydrogels (left) and GelMA ICC hydrogels (right) measured by parallel plate rheology. Each sample was tested three times.

GelMA bulk hydrogels showed rigid properties because of their irregular structure and smaller sized pores whereas GelMA ICC hydrogels showed compliant/compressible properties because of the interconnected, highly ordered macroporous structure and larger sized pores.

Rheological tests on the hydrogels were carried out to clarify the viscoelasticity of the hydrogels. At room temperature, both hydrogels displayed a predominantly elastic behavior as shown in Figures 3E, F. G′ was much higher than G″ at applied frequencies from .1 to 10 Hz, for both types of hydrogels. The storage modulus (G') of GelMA bulk hydrogels was 13.5 ± 1.8 kPa, and that of GelMA ICC hydrogels was 3.1 ± .2 kPa. The loss modulus (G") of GelMA bulk hydrogels was 1.6 ± .3 kPa and that of GelMA ICC hydrogels was .4 ± .1 kPa. Additionally, tan(δ) is generally used as a standard measure of the extent of viscous dissipation in a material. The tan(δ) value (.12) of GelMA bulk hydrogels was lower than of GelMA ICC hydrogels (.13), which suggests that ICC hydrogels have a more viscous character, which could improve the viscous dissipative ability of GelMA ICC hydrogels (Zhu et al., 2018).

From the compression and rheological test results, GelMA bulk hydrogels were stiffer than GelMA ICC hydrogels; Young's modulus of GelMA bulk hydrogels was 60 times higher than that of ICC hydrogels. ICC hydrogels showed a more viscous character compared with GelMA bulk hydrogels.

Degradation properties of different GelMA hydrogels

Despite the chemical modification of gelatin with MAA to prepare GelMA, GelMA still has a collagenase cleavage site (-R-Pro-X-Gly-Pro-R-, X; a neutral amino acid) (Klotz et al., 2016)

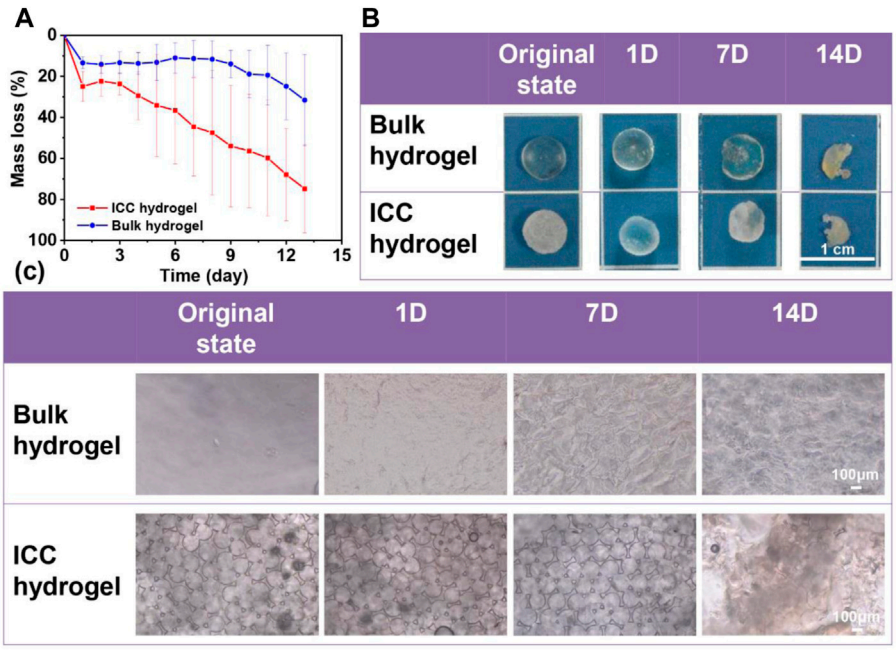

FIGURE 4
(A) Mass loss of GelMA bulk hydrogel (red line) and GelMA ICC hydrogel (black line) (n = 5; Mean ± S.D.) ($p < .0001$, one-way ANOVA, n = 5 measurements of two samples) **(B,C)** Gross images and microscopic images of degraded hydrogel samples at the fixed time points (original, 1D, 7D, and 14D). (For microscopic images taken by 10 × Lens, Scale bar is 100 μm).

Therefore in this study, the biodegradation properties of GelMA bulk and ICC hydrogels were demonstrated by 2 mg/mL collagenase ‖ (125 U/ml) at the pH 7.4 HBSS as a medium. From the results of Figure 4A, it is confirmed that the degradation rate of GelMA ICC hydrogels was much faster than that of GelMA bulk hydrogels due to their open macroporous structure that may facilitate collagenase ‖ diffusion inside the hydrogels. Other research results reported a similar phenomenon *in vivo*: porous silk scaffolds showed higher degradation rates than bulk materials due to the higher rates of enzyme diffusion into silk materials with higher porosity (Wang et al., 2008) GelMA ICC hydrogels lost almost half of their mass (44.6 ± 24.0%) at 7 days whereas GelMA bulk hydrogels lost less than half of their mass (35.9 ± 25.7%) after 14 days ($p < .0001$, one-way ANOVA, n = 5 measurements of two samples). For swelling measurement, some kind of errors could be generated in the process of wiping off the surface water on the hydrogels (especially ICC hydrogels that held a lot of water in the pores) and weighing them. From our previous research, the half-life of GelMA ICC with 98% DS was 4 h at 1 mg/mL collagenase ‖ (125 U/ml) (Lee et al., 2017). Our degradation employing a two times higher concentration of 2 mg/mL collagenase ‖ than in the previous research also showed a longer degradation time probably due to GelMA hydrogels with a higher crosslinking density resulted from use of highly substituted GelMA (around 300% DS). Also, Figure 4B, C show the real degradation images and morphological features respectively at designated time points. The gross images and surface morphological changes of GelMA bulk and ICC hydrogels were consistent with the mass loss results. With the degradation time proceeding, the surface of GelMA bulk hydrogels became rough, and the cavity rings of GelMA ICC hydrogels became disintegrated.

Biochemical characterization

RGD motif density of different 3D hydrogel systems

Besides the biophysical properties of GelMA hydrogels, their biochemical properties can play an important role in influencing cellular responses such as cell adhesion, viability, and morphology. GelMA has the tripeptide Arg-Gly-Asp (RGD) motifs that mediate cell attachment. Following Eqs 8–11, the Gap_{RGD} of GelMA ICC hydrogels was calculated to be about 3 nm whereas that of GelMA bulk hydrogels was calculated to be about 4 nm. Even though there are no significant differences between GelMA ICC and bulk hydrogel systems, a shorter distance of cell adhesion molecules in GelMA ICC hydrogels could be favorable for cell attachment compared to GelMA bulk hydrogels.

Cell viability and morphology in 3D hydrogel system

In this study, human dental pulp stem cells (hDPSCs) as model cells encapsulated in GelMA bulk hydrogels and GelMA ICC hydrogels were evaluated in terms of cell viability, proliferation, and morphology (Figures 5, 6). Firstly, we examined the loading efficiency of hDPSCs inside bulk and ICC hydrogels (Supplementary Figure S2). After 4 h culture, cell-laden hydrogel samples were transferred to a new culture plate to count the unloaded cell number and total loaded cell number. Two culture systems showed a similar loading efficiency of higher than 90%. In order to confirm the cell proliferation of each hydrogel system, the CCK-8 assay was conducted at 1, 7, and 21 days Figure 5A shows that the number of cells increased significantly in the ICC hydrogel system from day 1 to day 21, as compared with the bulk hydrogel system. Relative to the ICC hydrogel system, cells in the bulk hydrogel system marginally proliferated during the culture period of 21 days. Although GelMA is known to support good cell viability and proliferation (Loessner et al., 2016; Pepelanova et al., 2018; Xie et al., 2020), cell

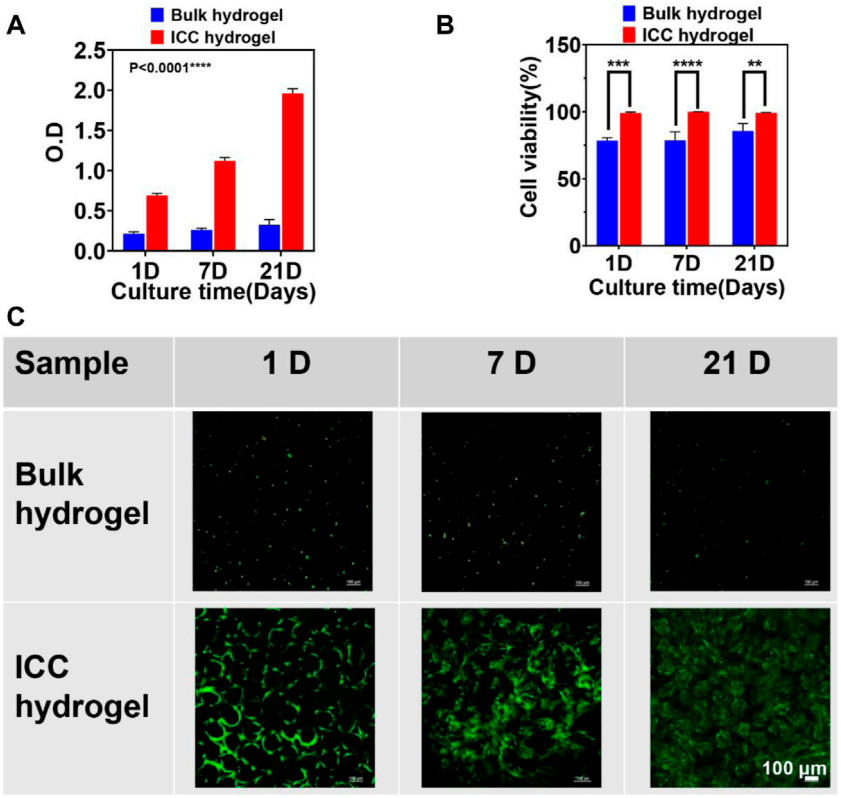

FIGURE 5
(A) Cell proliferation was evaluated by CCK-8 assay *via* measuring the absorbance at 450 nm in cell-laden GelMA bulk and ICC hydrogels on different culture times (1, 7, and 21 days) **(B)** Cell viability was calculated from live/dead staining images using the ImageJ software. **(C)** Images of Live/Dead staining cells on 1, 7, and 21 days were taken using a confocal microscope (10 × Lens, Scale bar is 100 μm). Live cells were stained with calcein-AM (green), and dead cells were stained with EthD-1 (red).

viability ad proliferation also depends on GelMA network structures. In this respect, GelMA ICC hydrogels with the interconnected macroporous structure could be more conducive to hDPSCs cell viability and proliferation when compared with the less porous bulk hydrogels. Also, the stiffness of GelMA bulk hydrogels that was 60 times higher than that of GelMA ICC hydrogels; the dense structure of the bulk hydrogels could limit nutrient absorption speed, affecting the cell viability, proliferation, and cell migration (Klotz et al., 2016). On the contrary, GelMA ICC hydrogels with the highly porous structure could support oxygen and nutrient supply and consequently improve cell viability and proliferation. Moreover, the cell viability of each sample was evaluated by Live/Dead assay. Live and dead cells were stained by green and red fluorescence under confocal microscope observation, respectively. As shown in Figure 5B, the bulk hydrogel system exhibited a cell viability of around 80% whereas GelMA ICC hydrogel system supported a high cell viability of around 100%. Some dead cells appeared in GelMA bulk hydrogels during the culture period (Supplementary Figure S3). In contrast to GelMA bulk hydrogels, GelMA ICC hydrogels exhibited only few dead cells across the cell culture period (Figure 5C). The macroporous ICC structure has been found to facilitate the transport of nutrients and oxygen in the scaffold (Hwang et al., 2010; Liaw et al., 2018).

The morphology of hDPSCs in GelMA bulk and ICC hydrogels was assessed by 4', 6-Diamidino-2-phenylindole dihydrochloride (DAPI for nucleus)/Alexa fluor 488-Phalloidin (for F-actin) staining at the set points of culture (Figure 6). Across the cell culture period, hDPSCs in the bulk hydrogels exhibited a round shape (Figure 7A) probably owing to the densely packed GelMA bulk hydrogel structure. It was reported that hDPSCs inside GelMA bulk hydrogels at a low concentration (<20 w/v%) and low DS (50%) exhibited a spindle shape (Luo et al., 2021) Increasing the GelMA concentration and degree of methacrylation leads to stiffer hydrogels with smaller pore sizes (Chen et al., 2012). In our research, GelMA bulk hydrogels with a higher concentration (30 w/v%) and higher DS (302%) showed much higher stiffness (~1.8 MPa), compared to the other GelMA system (~4.5 kPa) with a lower concentration (<20 w/v%) and lower (DS50%). Due to the high crosslinking density, the stiff GelMA bulk hydrogels can hamper cell spreading and migration. In comparison to those in the GelMA bulk hydrogels, hDPSCs in the ICC hydrogels made of the same GelMA displayed a spindle shape (Figure 6A). A cell in a 3D matrix initially exerts strains on the matrix, eliciting forces/stresses in response to this strain, as determined by the initial elastic modulus of the matrix; in an elastic matrix these forces are never relaxed, so that there is no remodeling of the matrix microenvironment; in a viscoelastic matrix, forces in the matrix can relax over time as a result of mechanical yielding and remodeling of the matrix (Chaudhuri et al., 2016). Therefore, the morphology of hDPSCs inside stiff and elastic bulk hydrogels maintained the original round shape. However, hDPSCs inside compliant and

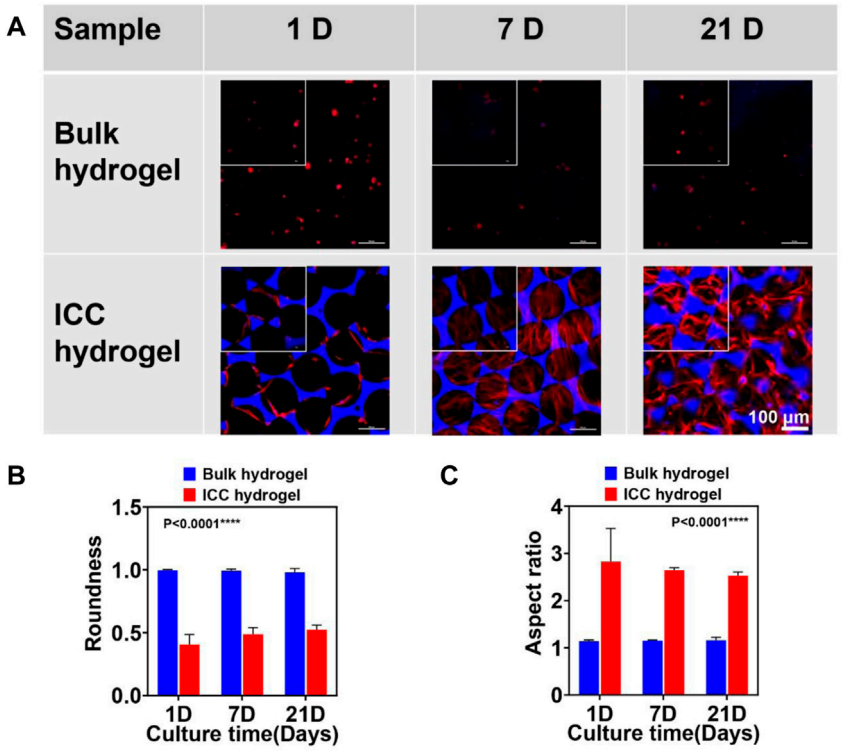

FIGURE 6
(A) Cell morphology in GelMA bulk and ICC hydrogels on different culture times (1, 7, and 21 days) confirmed *via* confocal microscopy. F-actin stained with Alexa Fluor 488 phalloidin (red) and nuclei stained with 4′, 6-Diamidino-2-phenylindole dihydrochloride (DAPI, blue). Large window images (20 × lens; scale bar is 100 μm). Small window images (40 × Lens, Scale bar is 100 μm) **(B,C)** Cell roundness and aspect ratio were calculated from confocal microscope images using ImageJ.

TABLE 1 A difference of GelMA bulk and ICC hydrogels in pore structure, physical properties, mechanical properties, and cell behaviors.

	GelMA bulk hydrogel	GelMA ICC hydrogel
Porous structure	Irregular	Regular
Pore Size (μm) (Freeze-dry state)	5.42 ± 1.90	99.80 ± 6.01
Ratio of pore (Freeze-dry state)	.73 ± .02%	.89 ± .01%
liquid absorption ability	Lower absorption	Higher absorption
Mechanical property	Stiff and brittle	Compliant and high compressible
Degradation	Slow	Fast
Cell viability	About 80%	About 100%
Proliferation	Slow	Fast
Cell Morphology	Round	Elongated
Advantages	Facile cell encapsulation	Excellent cell viability and Efficient exchange of oxygen, nutrients and wastes
Disadvantages	Limited cell proliferation/movement	Complex fabrication procedure

viscoelastic porous ICC hydrogels could easily remodel the ECM, leading to cell spreading. Figure 6B, C show the cell roundness and aspect ratio of hDPSCs in GelMA bulk hydrogels and ICC hydrogels. The cells in GelMA bulk hydrogels maintained the round shape across the entire cell culture time; their values of roundness and aspect ratio were around 1. However, In the case of GelMA ICC hydrogel system, the values of roundness and aspect ratio were over 1, indicating that cells spread on the matrix. Moreover, SEM images

clearly show that from both the surface or cross section views, round cell shapes in GelMA bulk and spindle cell shapes in GelMA ICC hydrogels were observed (Supplementary Figure S4). Interestingly, hDPSCs in GelMA ICC hydrogels appeared to interact with one another through the interconnected pores of ICC hydrogels, which is similar to the result of the previous 2D Monte Carlo (MC) simulations (Kim et al., 2016).

Conclusion

In this research, the structural influence of two different GelMA hydrogel systems on physical properties and cell behaviors was examined. Their differences are summarized in Table 1. Mechanical response and water absorption properties of both the hydrogel systems were significantly different, depending on their network structure. The sponge-like GelMA ICC hydrogels showed more highly compressible properties and higher water absorption ability compared to the bulk hydrogels. Additionally, GelMA ICC hydrogels with an interconnected macroporous structure resulted from using a monodisperse microbeads as a sacrificial template can enhance the cell infiltration, cell-cell interaction, and nutrients diffusion to enable tissue remodeling. On the other hand, stiff GelMA bulk hydrogels maintained the round morphology of cells, ICC hydrogels with a highly porous structure were applied as injectable platforms for the tissue engineering field because of their flexible and high water absorption properties (Bencherif et al., 2012; Zhu et al., 2016). In contrast to the ICC hydrogels, the bulk hydrogels are benign to *in situ* cell encapsulation process, and GelMA solutions can directly deliver cells and bioactive molecules to any type of tissue defects where GelMA solutions turn into therapeutic bulk hydrogels upon light irradiation, repairing the tissue (Zhao et al., 2016).

Data availability statement

The original contributions presented in the study are included in the article/Supplementary Material, further inquiries can be directed to the corresponding authors.

Author contributions

All authors listed have made a substantial, direct, and intellectual contribution to the work and approved it for publication.

Funding

This work was supported by Wenzhou Institute, University of Chinese Academy of Sciences (WIUCASQD2019003), the Zhejiang Provincial Natural Science Foundation of China (Grant No. LGF19E030001), the National Natural Science Foundation of China (32171316), the Wenzhou Major Scientific and Technological Innovation Key Medical and Health Project (Grant No. ZY2019010), and Zhejiang Provincial Natural Science Foundation of China (Grant No. LGF21H140007).

Conflict of interest

The authors declare that the research was conducted in the absence of any commercial or financial relationships that could be construed as a potential conflict of interest.

Publisher's note

All claims expressed in this article are solely those of the authors and do not necessarily represent those of their affiliated organizations, or those of the publisher, the editors and the reviewers. Any product that may be evaluated in this article, or claim that may be made by its manufacturer, is not guaranteed or endorsed by the publisher.

Supplementary material

The Supplementary Material for this article can be found online at: https://www.frontiersin.org/articles/10.3389/frsfm.2022.1101680/full#supplementary-material

References

Aisenbrey, E. A., and Murphy, W. L. (2020). Synthetic alternatives to Matrigel. *Nat. Rev. Mater* 5 (7), 539–551. doi:10.1038/s41578-020-0199-8

Andersen, T., Auk-Emblem, P., and Dornish, M. (2015). 3D cell culture in alginate hydrogels. *Microarrays (Basel)* 4 (2), 133–161. doi:10.3390/microarrays4020133

Annabi, N., Tamayol, A., Uquillas, J. A., Akbari, M., Bertassoni, L. E., Cha, C., et al. (2014). 25th anniversary article: Rational design and applications of hydrogels in regenerative medicine. *Adv. Mater.* 26, 85–124. doi:10.1002/adma.201303233

Bartosh, T. J., and Ylostalo, J. H. (2014). Preparation of anti-inflammatory mesenchymal stem/precursor cells (MSCs) through sphere formation using hanging-drop culture technique. *Curr. Protoc. Stem Cell. Biol.* 28, 2B. doi:10.1002/9780470151808.sc02b06s28

Bencherif, S. A., Sands, R. W., Bhatta, D., Arany, P., Verbeke, C. S., Edwards, D. A., et al. (2012). Injectable preformed scaffolds with shape-memory properties. *Proc. Natl. Acad. Sci.* 109 (48), 19590–19595. doi:10.1073/pnas.1211516109

Bertz, A., Wohl-Bruhn, S., Miethe, S., Tiersch, B., Koetz, J., Hust, M., et al. (2013). Encapsulation of proteins in hydrogel carrier systems for controlled drug delivery: Influence of network structure and drug size on release rate. *J. Biotechnol.* 163 (2), 243–249. doi:10.1016/j.jbiotec.2012.06.036

Caliari, S. R., and Burdick, J. A. (2016). A practical guide to hydrogels for cell culture. *Nat. Methods* 13 (5), 405–414. doi:10.1038/nmeth.3839

Chaudhuri, O., Gu, L., Klumpers, D., Darnell, M., Bencherif, S. A., Weaver, J. C., et al. (2016). Hydrogels with tunable stress relaxation regulate stem cell fate and activity. *Nat. Mater* 15 (3), 326–334. doi:10.1038/nmat4489

Chen, Y. C., Lin, R. Z., Qi, H., Yang, Y., Bae, H., Melero-Martin, J. M., et al. (2012). Functional human vascular network generated in photocrosslinkable gelatin methacrylate hydrogels. *Adv. Funct. Mater* 22 (10), 2027–2039. doi:10.1002/adfm.201101662

Choi, S. W., Zhang, Y., Macewan, M. R., and Xia, Y. (2013). Neovascularization in biodegradable inverse opal scaffolds with uniform and precisely controlled pore sizes. *Adv. Healthc. Mater* 2 (1), 145–154. doi:10.1002/adhm.201200106

Cukierman, E., Pankov, R., Stevens, D. R., and Yamada, K. M. (2001). Taking cell-matrix adhesions to the third dimension. *Science* 294 (5547), 1708–1712. doi:10.1126/science.1064829

da Silva, J., Lautenschlager, F., Sivaniah, E., and Guck, J. R. (2010). The cavity-to-cavity migration of leukaemic cells through 3D honey-combed hydrogels with adjustable internal dimension and stiffness. *BIOMATERIALS* 31 (8), 2201–2208. doi:10.1016/j.biomaterials.2009.11.105

Dehghani, F., and Annabi, N. (2011). Engineering porous scaffolds using gas-based techniques. *Curr. Opin. Biotechnol.* 22 (5), 661–666. doi:10.1016/j.copbio.2011.04.005

Dutta, R. C., and Dutta, A. K. (2009). Cell-interactive 3D-scaffold; advances and applications. *Biotechnol. Adv.* 27 (4), 334–339. doi:10.1016/j.biotechadv.2009.02.002

Huebsch, N., Lippens, E., Lee, K., Mehta, M., Koshy, S. T., Darnell, M. C., et al. (2015). Matrix elasticity of void-forming hydrogels controls transplanted-stem-cell-mediated bone formation. *Nat. Mater* 14 (12), 1269–1277. doi:10.1038/nmat4407

Hwang, C. M., Sant, S., Masaeli, M., Kachouie, N. N., Zamanian, B., Lee, S. H., et al. (2010). Fabrication of three-dimensional porous cell-laden hydrogel for tissue engineering. *Biofabrication* 2 (3), 035003. doi:10.1088/1758-5082/2/3/035003

Jaipan, P., Nguyen, A., and Narayan, R. J. (2017). Gelatin-based hydrogels for biomedical applications. *MRS Commun.* 7 (3), 416–426. doi:10.1557/mrc.2017.92

Jiang, S., Lyu, C., Zhao, P., Li, W., Kong, W., Huang, C., et al. (2019). Cryoprotectant enables structural control of porous scaffolds for exploration of cellular mechano-responsiveness in 3D. *Nat. Commun.* 10 (1), 3491. doi:10.1038/s41467-019-11397-1

Khayat, A., Monteiro, N., Smith, E. E., Pagni, S., Zhang, W., Khademhosseini, A., et al. (2017). GelMA-encapsulated hDPSCs and HUVECs for dental pulp regeneration. *J. Dent. Res.* 96 (2), 192–199. doi:10.1177/0022034516682005

Khetan, S., and Burdick, J. (2009). Cellular encapsulation in 3D hydrogels for tissue engineering. *J. Vis. Exp.* 32, 1590. doi:10.3791/1590

Kim, J. P., Li, C., Jin, H., Valluzzi, R., and Kaplan, D. L. (2004). Structure and properties of silk hydrogels. *Biomacromolecules* 5, 786–792. doi:10.1021/bm0345460

Kim, M. H., Kumar, S. K., Shirahama, H., Seo, J., Lee, J. H., Zhdanov, V. P., et al. (2016). Biofunctionalized hydrogel microscaffolds promote 3D hepatic sheet morphology. *Macromol. Biosci.* 16 (3), 314–321. doi:10.1002/mabi.201500338

Klotz, B. J., Gawlitta, D., Rosenberg, A., Malda, J., and Melchels, F. P. W. (2016). Gelatin-methacryloyl hydrogels: Towards biofabrication-based tissue repair. *Trends Biotechnol.* 34 (5), 394–407. doi:10.1016/j.tibtech.2016.01.002

Koshy, S. T., Ferrante, T. C., Lewin, S. A., and Mooney, D. J. (2014). Injectable, porous, and cell-responsive gelatin cryogels. *Biomaterials* 35 (8), 2477–2487. doi:10.1016/j.biomaterials.2013.11.044

Kotov, A. N., Liu, Y., Wang, S., Cumming, C., Eghtedari, M., Vargas, G., et al. (2004). Inverted colloidal crystals as three-dimensional cell scaffolds. *LANGMUIR* 20, 7887–7892. doi:10.1021/la049958o

Lee, B. H., Kim, M. H., Lee, J. H., Seliktar, D., Cho, N. J., and Tan, L. P. (2015). Modulation of Huh7.5 spheroid formation and functionality using modified PEG-based hydrogels of different stiffness. *PLoS One* 10 (2), e0118123. doi:10.1371/journal.pone.0118123

Lee, B. H., Shirahama, H., Kim, M. H., Lee, J. H., Cho, N. J., and Tan, L. P. (2017). Colloidal templating of highly ordered gelatin methacryloyl-based hydrogel platforms for three-dimensional tissue analogues. *NPG Asia Mater.* 9 (7), e412. doi:10.1038/am.2017.126

Li, J., and Mooney, D. J. (2016). Designing hydrogels for controlled drug delivery. *Nat. Rev. Mater* 1 (12), 16071. doi:10.1038/natrevmats.2016.71

Liaw, C. Y., Ji, S., and Guvendiren, M. (2018). Human tissue models: Engineering 3D hydrogels for personalized *in vitro* human tissue models (adv. Healthcare mater. 4/2018). *Adv. Healthc. Mater* 7 (4), 1870021. doi:10.1002/adhm.201870021

Liu, Y., Huang, Q., Wang, J., Fu, F., Ren, J., and Zhao, Y. (2017). Microfluidic generation of egg-derived protein microcarriers for 3D cell culture and drug delivery. *Sci. Bull.* 62 (18), 1283–1290. doi:10.1016/j.scib.2017.09.006

Loessner, D., Meinert, C., Kaemmerer, E., Martine, L. C., Yue, K., Levett, P. A., et al. (2016). Functionalization, preparation and use of cell-laden gelatin methacryloyl-based hydrogels as modular tissue culture platforms. *Nat. Protoc.* 11 (4), 727–746. doi:10.1038/nprot.2016.037

Long, T. J., Takeno, M., Sprenger, C. C., Plymate, S. R., and Ratner, B. D. (2013). Capillary force seeding of sphere-templated hydrogels for tissue-engineered prostate cancer xenografts. *Tissue Eng. Part C Methods* 19 (9), 738–744. doi:10.1089/ten.tec.2012.0388

Lu, Y. C., Song, W., An, D., Kim, B. J., Schwartz, R., Wu, M., et al. (2015). Designing compartmentalized hydrogel microparticles for cell encapsulation and scalable 3D cell culture. *J. Mater. Chem. B* 3 (3), 353–360. doi:10.1039/c4tb01735h

Luo, L., He, Y., Jin, L., Zhang, Y., Guastaldi, F. P., Albashari, A. A., et al. (2021). Application of bioactive hydrogels combined with dental pulp stem cells for the repair of large gap peripheral nerve injuries. *Bioact. Mater* 6 (3), 638–654. doi:10.1016/j.bioactmat.2020.08.028

Matai, I., Kaur, G., Seyedsalehi, A., McClinton, A., and Laurencin, C. T. (2020). Progress in 3D bioprinting technology for tissue/organ regenerative engineering. *Biomaterials* 226, 119536. doi:10.1016/j.biomaterials.2019.119536

McBeth, C., Lauer, J., Ottersbach, M., Campbell, J., Sharon, A., and Sauer-Budge, A. F. (2017). 3D bioprinting of GelMA scaffolds triggers mineral deposition by primary human osteoblasts. *Biofabrication* 9 (1), 015009. doi:10.1088/1758-5090/aa53bd

Naderi-Meshkin, H., Andreas, K., Matin, M. M., Sittinger, M., Bidkhori, H. R., Ahmadiankia, N., et al. (2014). Chitosan-based injectable hydrogel as a promising *in situ* forming scaffold for cartilage tissue engineering. *Cell. Biol. Int.* 38 (1), 72–84. doi:10.1002/cbin.10181

Nichol, J. W., Koshy, S. T., Bae, H., Hwang, C. M., Yamanlar, S., and Khademhosseini, A. (2010). Cell-laden microengineered gelatin methacrylate hydrogels. *Biomaterials* 31 (21), 5536–5544. doi:10.1016/j.biomaterials.2010.03.064

Nichols, J. E., Cortiella, J., Lee, J., Niles, J. A., Cuddihy, M., Wang, S., et al. (2009). *In vitro* analog of human bone marrow from 3D scaffolds with biomimetic inverted colloidal crystal geometry. *BIOMATERIALS* 30 (6), 1071–1079. doi:10.1016/j.biomaterials.2008.10.041

Pampaloni, F., Reynaud, E. G., and Stelzer, E. H. K. (2007). The third dimension bridges the gap between cell culture and live tissue. *Nat. Rev. Mol. Cell. Biol.* 8, 839–845. doi:10.1038/nrm2236

Parenteau-Bareil, R., Gauvin, R., and Berthod, F. (2010). Collagen-based biomaterials for tissue engineering applications. *Materials* 3 (3), 1863–1887. doi:10.3390/ma3031863

Pepelanova, I., Kruppa, K., Scheper, T., and Lavrentieva, A. (2018). Gelatin-methacryloyl (GelMA) hydrogels with defined degree of functionalization as a versatile toolkit for 3D cell culture and extrusion bioprinting. *Bioeng. (Basel)* 5 (3), 55. doi:10.3390/bioengineering5030055

Reif, R., Karlsson, J., Gunther, G., Beattie, L., Wrangborg, D., Hammad, S., et al. (2015). Bile canalicular dynamics in hepatocyte sandwich cultures. *Arch. Toxicol.* 89 (10), 1861–1870. doi:10.1007/s00204-015-1575-9

Santos, S. C., Custodio, C. A., and Mano, J. F. (2018). Photopolymerizable platelet lysate hydrogels for customizable 3D cell culture platforms. *Adv. Healthc. Mater* 7 (23), e1800849. doi:10.1002/adhm.201800849

Sedlačík, T., Nonoyama, T., Guo, H., Kiyama, R., Nakajima, T., Takeda, Y., et al. (2020). Preparation of tough double- and triple-network supermacroporous hydrogels through repeated cryogelation. *Chem. Mater.* 32 (19), 8576–8586. doi:10.1021/acs.chemmater.0c02911

Shanbhag, S., Woo Lee, J., and Kotov, N. (2005). Diffusion in three-dimensionally ordered scaffolds with inverted colloidal crystal geometry. *Biomaterials* 26 (27), 5581–5585. doi:10.1016/j.biomaterials.2005.01.059

Shao, C., Liu, Y., Chi, J., Wang, J., Zhao, Z., and Zhao, Y. (2019). Responsive inverse opal scaffolds with biomimetic enrichment capability for cell culture. *Res. (Wash D C)* 2019, 9783793. doi:10.34133/2019/9783793

Shirahama, H., Lee, B. H., Tan, L. P., and Cho, N. J. (2016). Precise tuning of facile one-pot gelatin methacryloyl (GelMA) synthesis. *Sci. Rep.* 6, 31036. doi:10.1038/srep31036

Stachowiak, A. N., and Irvine, D. J. (2008). Inverse opal hydrogel-collagen composite scaffolds as a supportive microenvironment for immune cell migration. *J. Biomed. Mater Res. A* 85 (3), 815–828. doi:10.1002/jbm.a.31661

Tang, Z., Chen, Q., Chen, F., Zhu, L., Lu, S., Ren, B., et al. (2018). General principle for fabricating natural globular protein-based double-network hydrogels with integrated highly mechanical properties and surface adhesion on solid surfaces. *Chem. Mater.* 31 (1), 179–189. doi:10.1021/acs.chemmater.8b03860

Van Den Bulcke, B. I., De Rooze, N., Schacht, E. H., Cornelissen, M., Cornelissen, M., and Berghmans, H. (2000). Structural and rheological properties of methacrylamide modified gelatin hydrogels. *biomacromolecules* 1 (1), 31–38. doi:10.1021/bm990017d

Wang, C. C., Yang, K. C., Lin, K. H., Wu, C. C., Liu, Y. L., Lin, F. H., et al. (2014). A biomimetic honeycomb-like scaffold prepared by flow-focusing technology for cartilage regeneration. *Biotechnol. Bioeng.* 111 (11), 2338–2348. doi:10.1002/bit.25295

Wang, J., Cheng, Y., Yu, Y., Fu, F., Chen, Z., Zhao, Y., et al. (2015). Microfluidic generation of porous microcarriers for three-dimensional cell culture. *ACS Appl. Mater Interfaces* 7 (49), 27035–27039. doi:10.1021/acsami.5b10442

Wang, K., Nune, K. C., and Misra, R. D. K. (2016). The functional response of alginate-gelatin-nanocrystalline cellulose injectable hydrogels toward delivery of cells and bioactive molecules. *Acta Biomater.* 36, 143–151. doi:10.1016/j.actbio.2016.03.016

Wang, L., Deng, F., Wang, W., Li, A., Lu, C., Chen, H., et al. (2018). Construction of injectable self-healing macroporous hydrogels via a template-free method for tissue engineering and drug delivery. *ACS Appl. Mater Interfaces* 10 (43), 36721–36732. doi:10.1021/acsami.8b13077

Wang, Y., Rudym, D. D., Walsh, A., Abrahamsen, L., Kim, H. J., Kim, H. S., et al. (2008). *In vivo* degradation of three-dimensional silk fibroin scaffolds. *Biomaterials* 29 (24-25), 3415–3428. doi:10.1016/j.biomaterials.2008.05.002

Welzel, P. B., Friedrichs, J., Grimmer, M., Vogler, S., Freudenberg, U., and Werner, C. (2014). Cryogel micromechanics unraveled by atomic force microscopy-based nanoindentation. *Adv. Healthc. Mater* 3 (11), 1849–1853. doi:10.1002/adhm.201400102

Welzel, P. B., Grimmer, M., Renneberg, C., Naujox, L., Zschoche, S., Freudenberg, U., et al. (2012). Macroporous starPEG-heparin cryogels. *BIOMACROMOLECULES* 13 (8), 2349–2358. doi:10.1021/bm300605s

Wendt, D., Riboldi, S. A., Cioffi, M., and Martin, I. (2009). Potential and bottlenecks of bioreactors in 3D cell culture and tissue manufacturing. *Adv. Mater* 21 (32-33), 3352–3367. doi:10.1002/adma.200802748

Wu, J., Zhao, Q., Sun, J., and Zhou, Q. (2012). Preparation of poly(ethylene glycol) aligned porous cryogels using a unidirectional freezing technique. *Soft Matter* 8 (13), 3620. doi:10.1039/c2sm07411g

Xie, M., Zheng, Y., Gao, Q., and He, Y. (2020). Facile 3D cell culture protocol based on photocurable hydrogels. *Bio-Design Manuf.* 4 (1), 149–153. doi:10.1007/s42242-020-00096-2

Yin, J., Yan, M., Wang, Y., Fu, J., and Suo, H. (2018). 3D bioprinting of low-concentration cell-laden gelatin methacrylate (GelMA) bioinks with a two-step cross-linking strategy. *ACS Appl. Mater Interfaces* 10 (8), 6849–6857. doi:10.1021/acsami.7b16059

Yue, K., Li, X., Schrobback, K., Sheikhi, A., Annabi, N., Leijten, J., et al. (2017). Structural analysis of photocrosslinkable methacryloyl-modified protein derivatives. *Biomaterials* 139, 163–171. doi:10.1016/j.biomaterials.2017.04.050

Yue, K., Trujillo-de Santiago, G., Alvarez, M. M., Tamayol, A., Annabi, N., and Khademhosseini, A. (2015). Synthesis, properties, and biomedical applications of gelatin methacryloyl (GelMA) hydrogels. *Biomaterials* 73, 254–271. doi:10.1016/j.biomaterials.2015.08.045

Zhang, Y. S., Cai, X., Yao, J., Xing, W., Wang, L. V., and Xia, Y. (2014). Non-invasive and *in situ* characterization of the degradation of biomaterial scaffolds by volumetric photoacoustic microscopy. *Angew. Chem. Int. Ed. Engl.* 53 (1), 184–188. doi:10.1002/anie.201306282

Zhang, Y. S., Regan, K. P., and Xia, Y. (2013). Controlling the pore sizes and related properties of inverse opal scaffolds for tissue engineering applications. *Macromol. Rapid Commun.* 34 (6), 485–491. doi:10.1002/marc.201200740

Zhao, X., Lang, Q., Yildirimer, L., Lin, Z. Y., Cui, W., Annabi, N., et al. (2016). Photocrosslinkable gelatin hydrogel for epidermal tissue engineering. *Adv. Healthc. Mater* 5 (1), 108–118. doi:10.1002/adhm.201500005

Zheng, J., Zhu, M., Ferracci, G., Cho, N. J., and Lee, B. H. (2018). Hydrolytic stability of methacrylamide and methacrylate in gelatin methacryloyl and decoupling of gelatin methacrylamide from gelatin methacryloyl through hydrolysis. *Macromol. Chem. Phys.* 219 (18), 1800266. doi:10.1002/macp.201800266

Zhu, M., Lin, S., Sun, Y., Feng, Q., Li, G., and Bian, L. (2016). Hydrogels functionalized with N-cadherin mimetic peptide enhance osteogenesis of hMSCs by emulating the osteogenic niche. *Biomaterials* 77, 44–52. doi:10.1016/j.biomaterials.2015.10.072

Zhu, M., Wang, Y., Ferracci, G., Zheng, J., Cho, N. J., and Lee, B. H. (2019). Gelatin methacryloyl and its hydrogels with an exceptional degree of controllability and batch-to-batch consistency. *Sci. Rep.* 9 (1), 6863. doi:10.1038/s41598-019-42186-x

Zhu, X., Chen, T., Feng, B., Weng, J., Duan, K., Wang, J., et al. (2018). Biomimetic bacterial cellulose-enhanced double-network hydrogel with excellent mechanical properties applied for the osteochondral defect repair. *ACS Biomaterials Sci. Eng.* 4 (10), 3534–3544. doi:10.1021/acsbiomaterials.8b00682